electronic materials

MDPI

Supplementary

Towards Sustainable Crossbar Artificial Synapses with Zinc-Tin Oxide

Carlos Silva [1], Jorge Martins [2,*], Jonas Deuermeier [2], Maria Elias Pereira [2], Ana Rovisco [2], Pedro Barquinha [2], João Goes [1], Rodrigo Martins [2], Elvira Fortunato [2] and Asal Kiazadeh [2,*]

[1] Department of Electrical and Computer Engineering, NOVA School of Science and Technology and CTS-UNINOVA, NOVA University Lisbon, Campus de Caparica, 2829-516 Caparica, Portugal; cmd.silva@campus.fct.unl.pt (C.S.); goes@fct.unl.pt (J.G.)

[2] i3N/CENIMAT, Department of Materials Science, NOVA School of Science and Technology and CEMOP/UNINOVA, NOVA University Lisbon, Campus de Caparica, 2829-516 Caparica, Portugal j.deuermeier@campus.fct.unl.pt (J.D.); mel.pereira@campus.fct.unl.pt (M.E.P.); a.rovisco@fct.unl.pt (A.R.); pmcb@fct.unl.pt (P.B.); rfpm@fct.unl.pt (R.M.); emf@fct.unl.pt (E.F.); a.kiazadeh@fct.unl.pt (A.K.)

* Correspondence: jds.martins@campus.fct.unl.pt (J.M.); a.kiazadeh@fct.unl.pt (A.K.)

The XRD pattern of ZTO thin film with two different thicknesses are shown in Figure S1. The absence of narrow peaks proves the amorphous nature of the material.

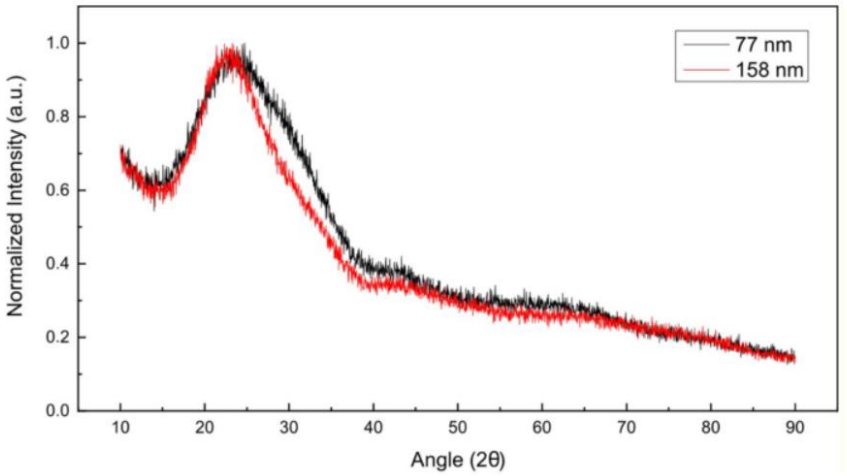


Figure S1. XRD characterization of the ZTO thin films.

Figure S2 shows the area-scaling of the patterned device (25 μm²) in comparison with the results of the non-patterned device (100 μm²) from a previous study [1].

Citation: Silva, C.; Martins, J.; Deuermeier, J.; Pereira, M.E.; Rovisco, A.; Barquinha, P.; Goes, J.; Martins, R.; Fortunato, E.; Kiazadeh, A. Towards Sustainable Crossbar Artificial Synapses with Zinc-Tin Oxide. *Electron. Mater.* **2021**, *2*, 105–115. https://doi.org/10.3390/electronic-mat2020009

Academic Editor: Anna Palau

Received: 18 March 2021
Accepted: 14 April 2021
Published: 16 April 2021

Publisher's Note: MDPI stays neutral with regard to jurisdictional claims in published maps and institutional affiliations.

Copyright: © 2021 by the authors. Submitted for possible open access publication under the terms and conditions of the Creative Commons Attribution (CC BY) license (http://creativecommons.org/licenses/by/4.0/).

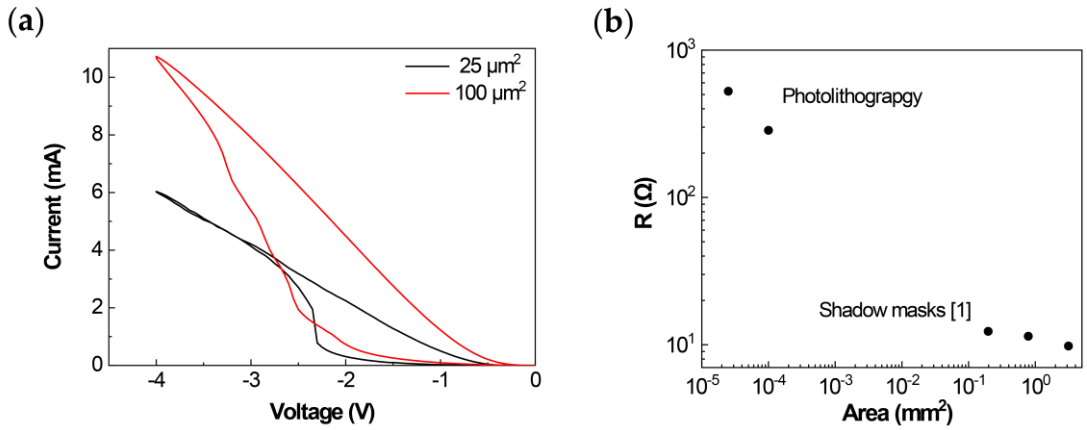


Figure S2. Area-scaling of the patterned device in comparison with the results of a previous study [1].

Figure S3 shows the dynamic retention properties of ZTO device when it is operated in 'forward set'. The memory retention loss of the device was fitted with a stretched-exponential function which has been already described in [2,3].The relaxation function is as follow:

$$\boldsymbol{\varphi(t) = I_0\, exp\left[-\frac{t}{\tau}\right]^{\beta}} \quad (1)$$

Where $\varphi(t)$ is the relaxation function, τ is the characteristic relaxation time, I_0 is initial current state, and β is the stretch index ($0 < \beta < 1$).

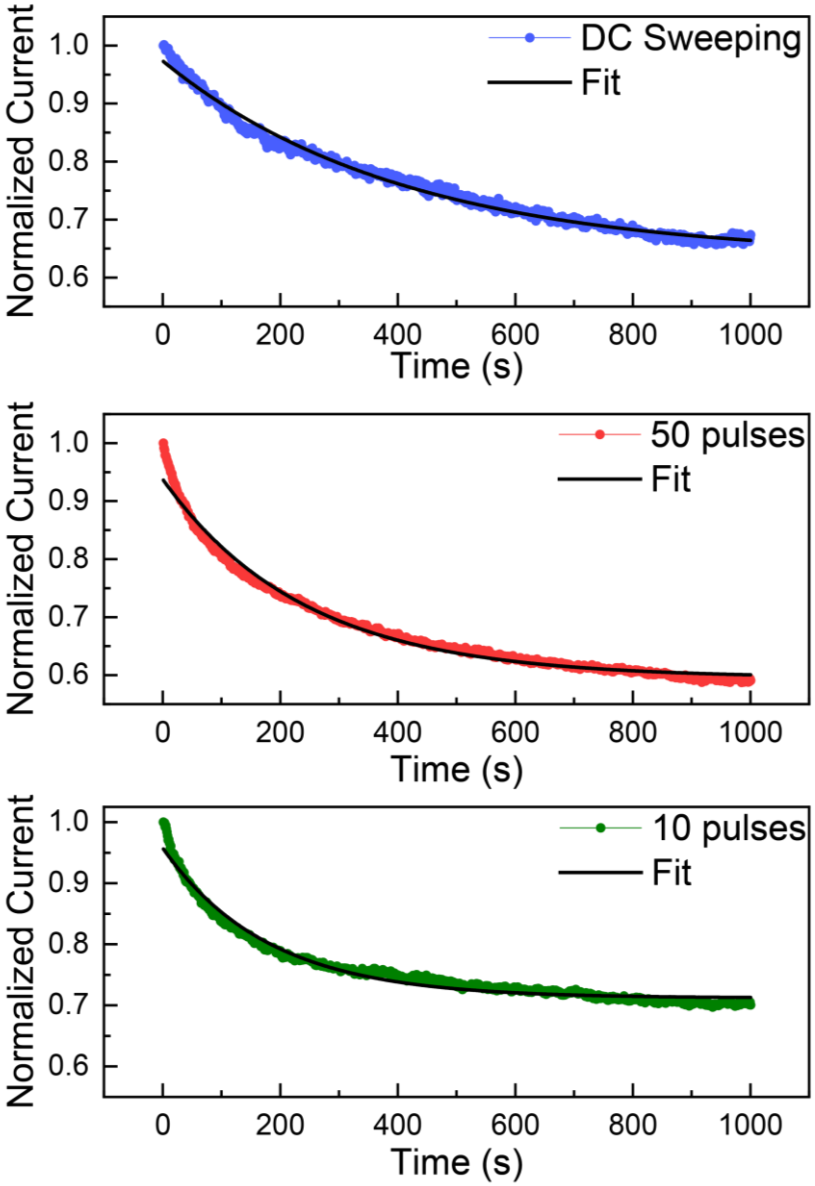


Figure S3. Typical dynamic retention time of the device after DC sweep set and 10 and 50 voltage pulses with an amplitude of -3 V and a width of 3 ms.

As verified by Table S1, the relaxation time characteristic is dependent on the operation method and number of pulses.

Table S1. Relaxation time characteristic associated with different SET operations.

Operation	DC Sweeping	50 Pulses	10 Pulses
τ	407.3 ± 4.8	240.8 ± 2.2	179.2 ± 2.0

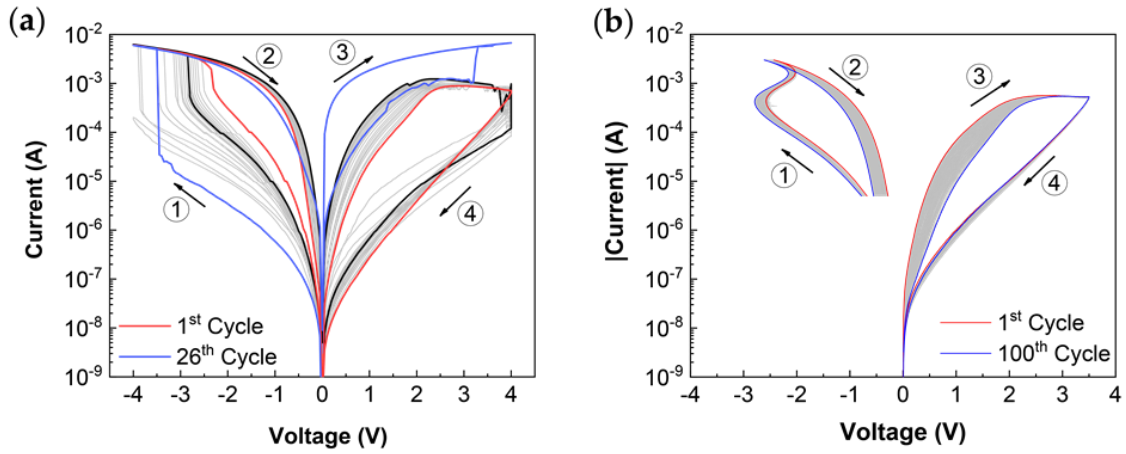


Figure S4. Current-controlled (**a**) and voltage-controlled (**b**) sweep cycles in semi-log scale.

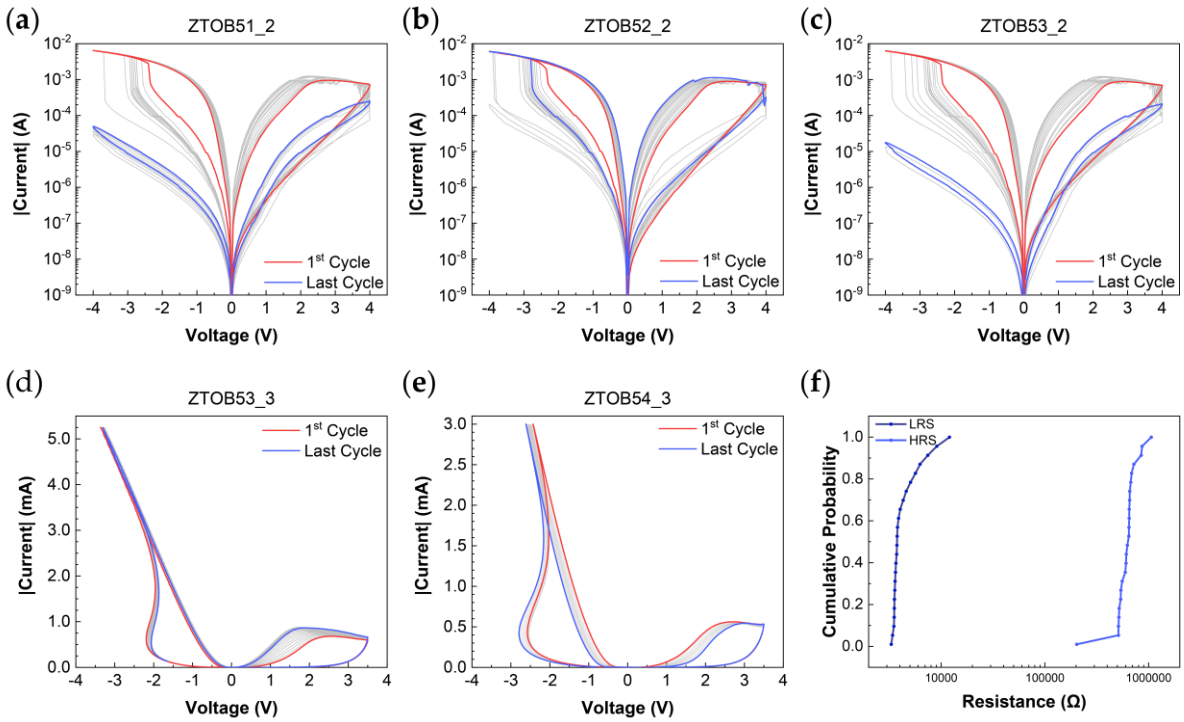


Figure S5. Typical device-to device variation in a row of devices with size of 25 μm² testing (**a–c**) under voltage sweeping and (**d**, **e**) current sweeping. (**f**) Cycle-to-cycle variation obtained from typical voltage-sweeping cycles.

For the high-resistance state (HRS) the conduction was found to follow Poole-Frenkel (P-F) Emission [4]. The current density is thus given by (1), in which $\boldsymbol{\mu}$ is the electron mobility, $\mathbf{N_C}$ is the effective density of states for electrons in the conduction band, E is the electric field, $\boldsymbol{\varepsilon_r}$ is the relative permittivity of ZTO, $\boldsymbol{\varepsilon_0}$ is the vacuum permittivity and $\boldsymbol{q\phi_t}$ is the energy level of the traps. Under this mechanism, the relationship (2) yields a linear dependency as is shown in Figure S6. The y-intercept of the fitted curves (y0) are this given by (3), from which the traps energy level was extracted (as 0.59 eV) as shown in Figure 4c of the main manuscript.

$$J = q\mu N_C E \cdot exp\left[-q\frac{\left(\phi_t - \sqrt{\frac{qE}{\pi\varepsilon_r\varepsilon_0}}\right)}{k_B T}\right] \quad (2)$$

$$\ln\left(\frac{J}{E}\right) - \sqrt{E} \tag{3}$$

$$y_0 = ln(\mathrm{q\mu N_C}) - \frac{q\phi_t}{k_B T} \tag{4}$$

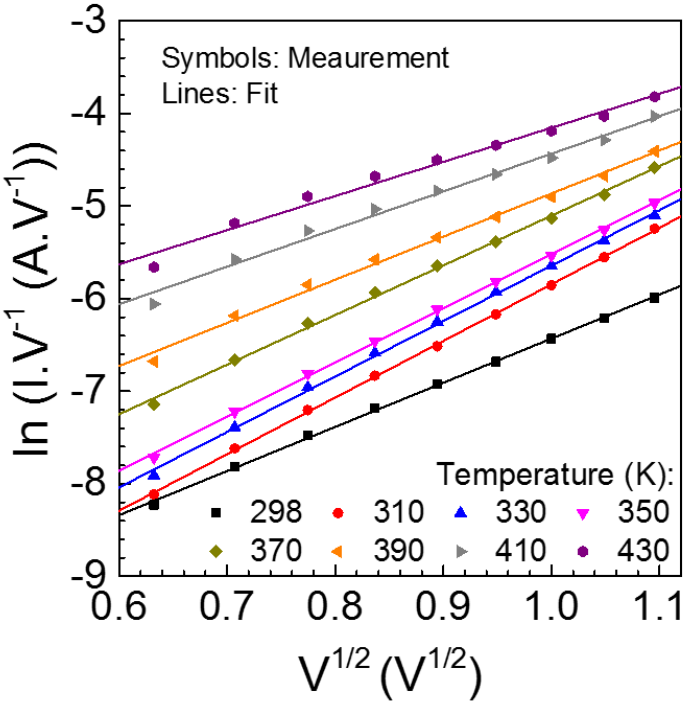


Figure S6. curves, and linear fitting, under the P-F emission.

References

1. Casa Branca, N.; Deuermeier, J.; Martins, J.; Carlos, E.; Pereira, M.; Martins, R.; Fortunato, E.; Kiazadeh, A. 2D Resistive Switching Based on Amorphous Zinc–Tin Oxide Schottky Diodes. *Adv. Electron. Mater.* **2020**, *6*, 1–8, doi:10.1002/aelm.201900958.
2. Pereira, M.; Deuermeier, J.; Nogueira, R.; Carvalho, P.A.; Martins, R.; Fortunato, E.; Kiazadeh, A. Noble-Metal-Free Memristive Devices Based on IGZO for Neuromorphic Applications. *Adv. Electron. Mater.* **2020**, 2000242, doi:10.1002/aelm.202000242.
3. Chang, T.; Jo, S.-H.; Lu, W. Short-Term Memory to Long-Term Memory Transition in a Nanoscale Memristor. *ACS Nano* **2011**, *5*, 7669–7676, doi:10.1021/nn202983n.
4. Chiu, F.-C. A Review on Conduction Mechanisms in Dielectric Films. *Adv. Mater. Sci. Eng.* **2014**, *2014*, 578168, doi:10.1155/2014/578168.